

# The Dimits Shift in a One-Field Fluid Model

Denis A. St-Onge<sup>1,2</sup> †

<sup>1</sup>Department of Astrophysical Sciences, Princeton University, Princeton, New Jersey 08544, USA

<sup>2</sup>Princeton Plasma Physics Laboratory, P.O. Box 451, Princeton, NJ 08543, USA

(Received 16 September 2018)

**Abstract.** The two-dimensional Terry-Horton equation is shown to exhibit the Dimits shift when suitably modified to capture both the nonlinear enhancement of zonal/drift-wave interactions and the existence of residual Rosenbluth-Hinton states. This phenomena persists through numerous simplifications of the equation, including a quasilinear approximation as well as a four-mode truncation. Analytic progress on the truncated system is reported, focused on determining the growth rates of zonal flows and calculating the upper bound of the Dimits shift. The results for the truncated system are then used to estimate the Dimits shift of the fully nonlinear system. A new understanding is thus developed on the fundamental nature of the Dimits shift, both on its operation and its eventual termination.

---

## 1. Introduction

The Dimits shift is the nonlinear upshift of the critical temperature gradient for the onset of turbulent transport witnessed in simulations of collisionless tokamak plasmas (Dimits et al., 2000). This results from the shearing away of turbulent radial streamers by poloidal zonal flows that are generated from the so-called secondary instability (Rogers et al., 2000). This shearing of radial streamers leads to fine-scale structure which is subsequently damped. The zonal flows are then able to persist on a longer time scale than the turbulent eddies, as they are not Landau-damped. These residual zonal flows are called Rosenbluth-Hinton states (Rosenbluth and Hinton, 1998), named for those who were the first to show this property. However, as the temperature gradient is further increased, the system eventually experiences a tertiary instability (Rogers et al., 2000), giving way to turbulent transport. While the qualitative aspects of the Dimits shift are understood, there is yet no technique that adequately calculates important quantities of the shift, such as its size. Understanding the essential aspects of this phenomenon is critical, as it is known that  $\mathbf{E} \times \mathbf{B}$  poloidal shear flows have the ability to suppress turbulence in physical systems. Such a mechanism is one candidate for explaining the L-H transition seen in tokamaks (Burrell, 1997). Being able to predict the saturated level of zonal flows and their effects on turbulence is crucial for the enhancement of plasma confinement.

The Dimits shift was first witnessed in gyrokinetic simulations of electrostatic

† E-mail address for correspondence: dstonge@princeton.edu

toroidal plasmas (Dimits et al., 1998), and was eventually demonstrated in nonlinear gyrofluid models with Landau-fluid closures (Beer and Hammett, 1998). This culminated in a landmark comparative study of various gyrokinetic and gyrofluid codes by Dimits et al. (2000). The shift has also been captured in some fluid models, using a variety of simplifications. One such model is the two-field Hasegawa-Wakatani model (studied separately by Numata et al. 2007 and Farrell and Ioannou 2009), which is a model that includes both ion-density-gradient drift waves and non-adiabatic electron effects. Another important model in the study of the Dimits shift has been the minimal two-field ion-temperature-gradient (ITG) mode, which retains both the ion continuity equation and an equation for the perpendicular ion temperature (Ottaviani et al., 1997; Kolesnikov and Krommes, 2005a,b).

Progress has been made into understanding the behaviour of the shift using both numerical simulation and analytical techniques, with much work focusing on the two-field Hasegawa-Wakatani and ITG systems. Numata et al. (2007) were able to show a sharp transition between steady turbulent states and relatively quiescent states dominated by zonal flows. However, their simulations had similar levels of viscous damping on both the drift-wave and zonal modes, which prevented them from making a connection to the steady Rosenbluth-Hinton states. They also made a prediction on the boundary of the shift using a stability analysis based on the Kelvin-Helmholtz instability, though the result greatly over-predicts the shift's size. Farrell and Ioannou (2009) used statistical closure techniques to clearly separate the dynamics of the zonal flows and of the drift-wave modes using a closure called the second-order cumulant expansion, or CE2. Here, the equations of motion are separated into zonally averaged and fluctuating parts, with eddy-eddy self-interaction terms being dropped in the fluctuation evolution equation. This closure is equivalent to a quasilinear system when ergodicity is assumed. They were able to demonstrate that the essential physical effects are captured even without the eddy-eddy self-interactions. As the drift-wave and zonal equations are also separated, they were able to use a physically relevant frictional zonal damping (as would result from ion-ion collisions, see Lin et al. 1999) that was distinct from the drift-wave damping. However, their simulations were also stochastically forced to imitate the homogeneous turbulence lost upon neglecting the eddy-eddy self-interactions. This approach is invalid when studying the Dimits shift, however, as there is no turbulence in this regime, thus they were not able to observe a Dimits shift.

Analytical work has also been done using the minimal two-field toroidal ITG model. Kolesnikov and Krommes (2005a,b) were able to calculate the Dimits shift of a four-mode truncated system (4MT) using the tools of dynamical systems. However, the size of the shift was found to be strongly dependent on the truncation number of the system. Additionally, the system failed to saturate beyond the Dimits shift. This model has also been studied under the CE2 framework by St-Onge and Krommes (2017), in which the effect of discrete-particle noise on the onset of zonostrophic instability was studied. Even for such a simple two-field system, the CE2 results in a system of five quantities (two zonal-averaged fields and three independent components of a covariance tensor with the off-diagonal component being complex) and even the simplest of linear calculations can quickly become tedious. It is worth noting here that the two-field ITG model also suffers a flaw in that, beyond the point of linear instability, the eigenvalues of the system become purely imaginary and the system ceases to exhibit any linear wave physics, such as dispersion. It will be shown herein that dispersive effects can play an important

role on the behaviour of the Dimits shift. In addition, both the Hasegawa-Wakatani and minimal two-field ITG systems are non-normal, and as a result can be made to exhibit subcritical turbulence, a phenomena that can obfuscate the essential physics of drift waves and zonal flows.

What, then, is the simplest model that exhibits the Dimits shift with a minimal amount of physics? To be successful, the model must

- (a) contain a nonlinear boost in zonal flow interactions. This would enable efficient energy transfer between zonal and non-zonal modes, leading to the quenching of turbulence through the shearing of eddies;
- (b) allow for the existence of steady states consisting purely of zonal modes. For these solutions to be proper steady states, zonal modes would necessarily be linearly undamped;
- (c) exhibit a finite Dimits shift. In other words, given a sufficient amount of linear drive, steady zonal states must give way to turbulence leading to a finite amount of turbulent transport;
- (d) have the ability for saturation beyond the Dimits shift without the need for zonal damping. Otherwise, saturated states may depend on the amount of zonal damping, in contrast with the original numerical studies of Dimits et al. (2000).

The goal of this article, then, is to show that the Terry-Horton equation can be made to exhibit all four traits with reasonable physically-motivated modifications. This equation will henceforth be referred to as the modified Terry-Horton Equation (mTHE). I shall also show that various simplifications of this equation also exhibit the four properties. These simplifications will be used to gain insight into how the energy transfer by zonal modes is different than the usual Kolmogorov-type cascade, as well as how the termination of the Dimits shift is related to the destabilization of well-coupled modes. Using this insight, I shall show how one can estimate the size of the Dimits shift for the fully nonlinear system in a way that elucidates the fundamental aspects of the shift's mechanism.

The remainder of this article is organized as follows. In Sec. 2 I describe the historically important models that lead up to the mTHE, which is described in Sec. 3. In Sec. 4 I demonstrate by direct numerical simulation that the mTHE exhibits the Dimits shift. Analytical results are presented in Sec. 5, starting with analysis of the 4MT, followed by an estimation of the size of the Dimits shift for the nonlinear system. This is done in Sec. 5.3. Finally, the work is summarized in Sec. 6.

## 2. Review

### 2.1. The (Modified) Hasegawa-Mima Equation

The paradigmatic model for density-gradient-driven drift waves is the Hasegawa-Mima equation (HME), which captures  $\mathbf{E} \times \mathbf{B}$  advection of the electrostatic potential caused linearly by background ion-density gradients and nonlinearly by density fluctuations on a local segment of the bad-curvature side near the midplane. The system is two-dimensional in that it neglects any toroidal variation in the electrostatic potential (i.e.  $k_{\parallel} \ll k_{\perp}$ ); thus the fields can be described with just radial and poloidal coordinates.

The HME is given by

$$\partial_t \zeta + \mathbf{v} \cdot \nabla \zeta - \beta \partial_y \varphi = 0, \quad (2.1)$$

where  $\mathbf{v} = (-\partial_y \varphi, \partial_x \varphi)$  is the  $\mathbf{E} \times \mathbf{B}$  drift velocity,  $\beta \doteq a/L_n$  parameterizes the density gradient,  $L_n^{-1} = -d \ln n_0 / dr$  is the background density gradient scale length,

$$\zeta = (\nabla_{\perp}^2 - 1)\varphi \quad (2.2)$$

is the generalized vorticity, derived from the gyrokinetic Poisson equation with adiabatic electron response, and  $\varphi \doteq (e\phi/T_e)(a/\rho_s)$  is the dimensionless perturbation to the electrostatic potential. Throughout this paper, time and space are normalized by  $a/c_s$  and  $\rho_s$ , respectively, where  $a$  is the minor radius,  $\rho_s \doteq c_s/\omega_{ci}$  is the sound radius, and  $c_s \doteq (ZT_e/m_i)^{1/2}$  is the sound speed. Coordinates are in a local Cartesian grid where  $x$  represents the radial coordinate and  $y$  represents the poloidal coordinate. The operator  $\nabla_{\perp}$  denotes the gradient perpendicular to the magnetic field, which acts in the  $x$  and  $y$  direction for this particular setup. For any function  $f$ ,

$$\mathbf{v} \cdot \nabla f = \frac{\partial \varphi}{\partial x} \frac{\partial f}{\partial y} - \frac{\partial \varphi}{\partial y} \frac{\partial f}{\partial x} \equiv \{\varphi, f\} \quad (2.3)$$

which defines the Poisson Bracket  $\{\cdot, \cdot\}$ .

The nonlinear interaction of the HME conserves two quadratic invariants. These are the energy density

$$\mathcal{E} \doteq \frac{1}{L_x L_y} \int_0^{L_x} dx \int_0^{L_y} dy \frac{1}{2} [(\nabla_{\perp} \varphi)^2 + \varphi^2], \quad (2.4)$$

and the generalized enstrophy density

$$\mathcal{Z} \doteq \frac{1}{L_x L_y} \int_0^{L_x} dx \int_0^{L_y} dy \frac{1}{2} \zeta^2. \quad (2.5)$$

Because the HME is a two-dimensional equation with two nonlinearly conserved quantities, the system experiences a dual cascade where injected energy at some intermediate scale simultaneously causes a flow of energy to larger scales and a flow of enstrophy to smaller scales. Note that conservation of the generalized enstrophy  $\mathcal{Z}$  is a direct result of the nonlinear interaction being in the form of a Poisson bracket and does not depend on the specific form of  $\zeta$  given by (2.2). This is important for the Terry-Horton equation, which will be discussed in Sec. 2.2.

One shortcoming of the HME is that it does not capture the correct zonal flow physics as seen in more complete gyrokinetic simulations (Hammett et al., 1993). This stems from how one derives the adiabatic electron response. In the HME, this is done via parallel force balance in the electron momentum equation:

$$-en_e E_{\parallel} - \nabla_{\parallel} P_e = 0. \quad (2.6)$$

where  $E_{\parallel}$  is the electric field parallel to the magnetic field,  $n_e$  and  $P_e$  are respectively the electron density and pressure, and  $\nabla_{\parallel}$  is the gradient along the magnetic field ( $\nabla_{\parallel} \equiv \partial_z$  for HME). Assuming isothermal electrons, this leads to

$$\nabla_{\parallel} (\varphi - \delta n_e) = 0 \quad (2.7)$$

in dimensionless units. This has the solution

$$\delta n_e = \varphi + C, \quad (2.8)$$

where  $C$  is constant along the magnetic field. Naively, one could set this constant to zero and arrive at the HME. However, to correctly determine the value of  $C$ , one must use an additional constraint.

Physically, electrons that evolve adiabatically will experience no radial transport, so the density perturbation averaged over a flux surface must vanish. This leads to  $C = -\langle\varphi\rangle_\psi$ , or

$$\delta n_e = \varphi - \langle\varphi\rangle_\psi, \quad (2.9)$$

where  $\langle\dots\rangle_\psi$  denotes the flux-surface average. In two dimensions, this is equivalent to the zonal average  $\langle f\rangle$ ,

$$\langle f\rangle \doteq \frac{1}{L_y} \int_0^{L_y} dy f. \quad (2.10)$$

Equation (2.2) is thus modified to now read

$$\zeta = \nabla_\perp^2 \varphi - \varphi + \langle\varphi\rangle \doteq (\nabla_\perp^2 - \hat{\alpha})\varphi, \quad (2.11)$$

where  $\hat{\alpha}$  is an operator that is zero when acting on zonal modes and is unity otherwise.

The Hasegawa-Mima equation that uses this form of the modified vorticity is referred to as the modified-Hasegawa-Mima equation (mHME). While the nonlinear interaction is changed by this new Poisson equation, it still conserves both the energy density  $\mathcal{E}$  and the generalized vorticity density  $\mathcal{Z}$ , where  $\zeta$  in  $\mathcal{Z}$  is now given by (2.11). It is helpful to define the zonal ( $k_y = 0$ ) and drift-wave ( $k_y \neq 0$ ) energy densities,

$$\mathcal{E}^{\text{ZF}} = \frac{1}{L_x} \int_0^{L_x} dx \frac{1}{2} \partial_x \langle\varphi\rangle^2, \quad (2.12)$$

$$\mathcal{E}^{\text{DW}} = \frac{1}{L_x L_y} \int_0^{L_x} dx \int_0^{L_y} dy \frac{1}{2} [(\nabla_\perp \varphi')^2 + \varphi'^2], \quad (2.13)$$

where  $\varphi' = \varphi - \langle\varphi\rangle$ . These quantities will be helpful when determining whether a system is in a zonal-flow-dominated state or a turbulence-dominated state, and will be later used in Sec. 4.2.

Both the HME and the mHME have been extensively studied in terms of both the modulational instability (Connaughton et al., 2010), which concerns the instability of background drift wave to a zonal flow, and the more general zonostrophic instability (Parker and Krommes, 2013, 2014; Srinivasan and Young, 2012) which encompasses the instability of *any* statistically homogeneous steady state (including steady states of single realizations) to a zonal flow.

## 2.2. The Terry-Horton Equation

Another shortcoming of the HME is the lack of irreversibility. Studies of the HME usually add dissipation by hand and are stochastically forced to drive the system. An alternative to adding forcing is to include destabilizing effects in the electron response obtained from kinetic theory. These effects materialize most simply as an additional non-Hermitian operator  $\hat{\delta}$  in the Poisson equation (2.2), resulting in

$$\zeta = (\nabla_\perp^2 + i\hat{\delta} - 1)\varphi, \quad (2.14)$$

or

$$\hat{\zeta} = -(k_\perp^2 - i\hat{\delta}_k + 1)\hat{\varphi} \quad (2.15)$$

when Fourier transformed. Here,  $\widehat{\delta}_{\mathbf{k}}$  is a real variable that depends on the wavevector  $\mathbf{k}$ . The resulting system is named the Terry-Horton Equation (THE) and has been extensively studied (Terry and Horton, 1983, 1982). It has, however, fallen out of favour with respect to the more rigorously derived Hasegawa-Wakatani system, which has now become the standard system of equations for dealing with linearly unstable drift waves in a two-field fluid system.

The non-adiabatic part of the electron response  $\widehat{\delta}_{\mathbf{k}}$  for the THE can be chosen to describe various types of physical mechanisms. As an example, for the untrapped collisionless electron-wave resonance, one has in physical units (Tang, 1978)

$$i\delta_{\mathbf{k}} = i(\pi/2)^{1/2} \left[ \omega_{\mathbf{k}} - \omega_{*e} \left( 1 - \frac{1}{2}\eta_e \right) \right] / |k_{\parallel}| v_{\text{the}}, \quad (2.16)$$

where  $\omega_{*e} \doteq ck_y T_e / e B_0 L_n$  is the electron diamagnetic drift frequency, and  $\eta_e \doteq d \ln T_e / d \ln n_0$ . To proceed,  $\omega_{\mathbf{k}}$  is taken to be the frequency of the linearized HME. Then, in dimensionless units,

$$i\widehat{\delta}_{\mathbf{k}} = i\delta_0 k_y \left( \frac{k_{\perp}^2}{1 + k_{\perp}^2} - \frac{1}{2}\eta_e \right), \quad (2.17)$$

where  $\delta_0 = (\pi/2)^{1/2} (m_e/m_i)^{1/2} / |k_{\parallel}| L_n$  is a constant of order unity that parameterizes the parallel wavenumber  $k_{\parallel}$  (as  $L_n$  is already parameterized by  $\beta$ ). One arrives at the original form of  $\widehat{\delta}_{\mathbf{k}} = \delta_0 k_y (k_{\perp}^2 - \eta_e/2)$  given in Terry and Horton (1983) by taking the long-wavelength ( $k_{\perp}^2 \ll 1$ ) limit. As another example, for trapped collisional electron dynamics,

$$i\widehat{\delta}_{\mathbf{k}} = i\delta_0 k_y, \quad (2.18)$$

where  $\delta_0 = \eta_e (\epsilon/2)^{1/2} (6/\pi^{1/2}) / \nu_{\text{eff}}$  is a constant of order unity,  $\epsilon$  is the inverse aspect ratio and  $\nu_{\text{eff}}$  is the collisional detrapping rate. A thorough review of such mechanisms is given in Tang (1978).

In addition to instability, the THE equation introduces non-zero particle transport. For instance, if one takes the non-adiabatic electron response to be simply  $i\widehat{\delta}_{\mathbf{k}} = ik_y$ , one obtains a particle flux

$$\Gamma_n \doteq \int dx dy v_x \delta n_i = \int dx dy \zeta \partial_y \varphi = \int dx dy (\partial_y \varphi)^2, \quad (2.19)$$

which is positive-definite. Another important distinction of the THE is that it has only one nonlinearly conserved quantity, the generalized vorticity  $\zeta$ , which can alter the system's ability to experience a dual-cascade. For instance,  $\widehat{\delta}_{\mathbf{k}}$  as given by (2.18) becomes much larger relative to  $\nabla_{\perp}^2$  at large scales, leading to degeneracy between  $\mathcal{E}$  and  $\mathcal{Z}$ . This has been shown by Liang et al. (1993) to disable the dual cascade. However,  $\widehat{\delta}_{\mathbf{k}}$  as given by (2.17) is small relative to  $\nabla_{\perp}^2$  at both small and large scales, thus for this type of system the dual cascade is expected to remain prevalent.

### 3. The Modified Terry-Horton Equation

#### 3.1. Description

The model that is the focus of this article is a modified version of the THE that is designed to capture the essential zonal physics found in gyrokinetic simulations. The resulting system is hence referred to as the modified Terry-Horton Equation

(mTHE), and is given by

$$\frac{\partial \zeta}{\partial t} + \mathbf{v} \cdot \nabla \zeta = \beta \frac{\partial \varphi}{\partial y} - \hat{\alpha} D \zeta, \quad (3.1)$$

where  $\mathbf{v} = (-\partial_y \varphi, \partial_x \varphi)$  and

$$\hat{\zeta} = -(k_\perp^2 - i\hat{\delta}_\mathbf{k} + \hat{\alpha}_\mathbf{k})\hat{\varphi}. \quad (3.2)$$

in Fourier space. Here,  $D$  is a damping operator that, in Fourier space, is assumed to be even in both  $k_x$  and  $k_y$ . This model contains two modifications to the original THE. First, the adiabatic electron response is modified to ensure that electrons do not respond to a potential that is constant along a flux surface. This results in an enhancement of the zonal interaction between drift waves in the nonlinear term. The second modification is the appearance of the  $\hat{\alpha}$  operator in front of the damping term, which ensures that only the drift-wave modes ( $k_y \neq 0$ ) are linearly damped. By doing so, the mTHE is made to model the residual Rosenbluth-Hinton zonal states (Rosenbluth and Hinton, 1998) witnessed in the simulations performed in Dimits et al. (2000). As a result, any state that consists purely of zonal flows is a steady-state solution to (3.1). The damping on the drift waves can then be interpreted to be related to Landau damping of the potential fluctuation. As this is a fluid model, it is agnostic to the eventual fate of the fine-scale velocity-space structure that would result in the ion distribution function.

One may also add a separate damping component to the zonal flows, as was done in Lin et al. (1999). This typically results in bursty behaviour involving transitions between zonally dominated states and turbulence-dominated states within what would normally be the region of the Dimits shift. While this phenomena is interesting in its own right, it is not touched upon in this article.

A question that should be raised is whether or not adding non-adiabatic effects to the electron response will also require modification to the constant of integration when solving the parallel electron force balance. For the remainder of the paper, however, I shall assume that these non-adiabatic effects are sufficiently small as to not destroy good flux surfaces. Thus, electrons will continue to not respond to a potential that is constant along a flux surface. Finally, I require that the flux-surface average of the non-adiabatic electron response  $\langle i\hat{\delta}_\mathbf{k} \rangle_\psi = 0$ , which is the case for the examples noted in Sec. 2.2. This is akin to saying that the background density gradients lie in the radial direction.

### 3.2. Linear Properties

The eigenvalues of (3.1) for the linearization around the zero state can be readily calculated. For drift-wave modes, the growth rates and frequencies for a time dependence of  $e^{\lambda_\mathbf{k} t}$  where  $\lambda_\mathbf{k} = \gamma_\mathbf{k} - i\omega_\mathbf{k}$  are, respectively,

$$\gamma_\mathbf{k} = -D_\mathbf{k} + \frac{\beta k_y \hat{\delta}_\mathbf{k}}{(1 + k_\perp^2)^2 + \hat{\delta}_\mathbf{k}^2}, \quad (3.3)$$

$$\omega_\mathbf{k} = \frac{\beta k_y (1 + k_\perp^2)}{(1 + k_\perp^2)^2 + \hat{\delta}_\mathbf{k}^2}. \quad (3.4)$$

For zonal modes, both are identically zero by construction, as I've neglected collisional damping.

### 3.3. Quasilinear Model

I also consider numerous approximations to (3.1). The typical first step is to decompose the modified vorticity into zonal and non-zonal components, viz.  $\zeta = \langle \zeta \rangle + \zeta'$ . By zonally averaging (3.1) and subtracting the result from the original equation, one obtains the new system of equations

$$\frac{\partial \zeta'}{\partial t} = -U \frac{\partial \zeta'}{\partial y} - u' \frac{\partial^2 U}{\partial x^2} + \beta \frac{\partial \varphi'}{\partial y} + D\zeta' - F', \quad (3.5a)$$

$$\frac{\partial U}{\partial t} = -\frac{\partial}{\partial x} \langle u'v' \rangle - (\langle u'\widehat{\delta}\varphi' \rangle - \langle\langle u'\widehat{\delta}\varphi' \rangle\rangle), \quad (3.5b)$$

where  $u' \doteq -\partial_y \varphi'$ ,  $v' \doteq \partial_x \varphi'$ ,  $U(x) \doteq \partial_x \langle \varphi \rangle$  is the zonal velocity,  $F' \doteq \{\varphi', \zeta'\} - \langle \{\varphi', \zeta'\} \rangle$ , and  $\langle\langle \dots \rangle\rangle$  denotes the total spatial average. The last term in (3.5b) results from integrating in  $x$  to arrive at the equation for zonal velocity and is chosen to ensure mathematical consistency for  $k_x = 0$ . So far, this is an exact description of the original equation (3.1). One arrives at the quasilinear system (QL) when the eddy-eddy interactions in the fluctuation equation (3.5a) are neglected. This is done by simply setting  $F' = 0$ .

The physical effects that the quasilinear equations neglect are the eddy-eddy self-interactions. However, they do retain the eddy-eddy interactions that act on zonal modes, which appear in the form of a Reynolds stress (first term on the right-hand side of (3.5b)), as well as a term unique to the Terry-Horton equation (second term on the right-hand side of (3.5b)). For the model  $\widehat{\delta}_{\mathbf{k}}$  given by (2.17), this term describes radial  $\mathbf{E} \times \mathbf{B}$  advection of the background electron gradients. It has already been shown that these interactions play a dominant role in the creation of zonal flows (Parker and Krommes, 2013), as well as in catalyzing the transfer of energy from large-scale drift-wave modes to smaller scales (Farrell and Ioannou, 2009), which are subsequently damped.

### 3.4. Four-Mode Truncation

Previous work on the HME and the two-field ITG model has concentrated on low-order Galerkin truncations, focusing on the modulational instability of a single mode to calculate zonal-flow growth rates, as well as on calculating the Dimits shift using the tools of dynamical systems (Kolesnikov and Krommes, 2005a,b). To connect this article to this previous work, I formulate a four-mode truncation (4MT) of (3.1); in Fourier space,

$$\begin{aligned} \frac{\partial \varphi_{\mathbf{k}}}{\partial t} = & (\gamma_{\mathbf{k}} - i\omega_{\mathbf{k}})\varphi_{\mathbf{k}} + \frac{1}{\widehat{\alpha}_{\mathbf{k}} - i\widehat{\delta}_{\mathbf{k}} + k_{\perp}^2} \sum_{\mathbf{k}_1, \mathbf{k}_2} k_{1x} k_{2y} \varphi_{\mathbf{k}_1} \varphi_{\mathbf{k}_2} \\ & \times \delta_{\mathbf{k}-\mathbf{k}_1-\mathbf{k}_2} [\widehat{\alpha}_{\mathbf{k}_2} - \widehat{\alpha}_{\mathbf{k}_1} - i(\widehat{\delta}_{\mathbf{k}_2} - \widehat{\delta}_{\mathbf{k}_1}) + k_{2\perp}^2 - k_{1\perp}^2]. \end{aligned} \quad (3.6)$$

In the 4MT, I retain a pure drift-wave mode  $\mathbf{p} = (0, p_y)$ , a pure zonal mode  $\mathbf{q} = (q_x, 0)$ , and two sidebands  $\mathbf{r}_{\pm} = (\pm q_x, p_y)$ . In addition, the complex conjugate modes are retained in order to satisfy the reality condition. I also assume that  $\widehat{\delta}_{\mathbf{r}_-} = \widehat{\delta}_{\mathbf{r}_+} = \widehat{\delta}_{\mathbf{r}}$ , which is the case for the two examples of  $\widehat{\delta}_{\mathbf{k}}$  given in Sec. 2.2. Finally,  $\widehat{\alpha}_{\mathbf{q}}$  is kept arbitrary to compare with previous results.



The resulting set of equations is

$$\partial_t \varphi_{\mathbf{p}} = (\gamma_{\mathbf{p}} - i\omega_{\mathbf{p}})\varphi_{\mathbf{p}} + M_{\mathbf{p}}(\varphi_{\mathbf{r}_-}\varphi_{\mathbf{q}} - \varphi_{\mathbf{r}_+}\varphi_{\mathbf{q}}^*), \quad (3.7a)$$

$$\partial_t \varphi_{\mathbf{r}_+} = (\gamma_{\mathbf{r}} - i\omega_{\mathbf{r}})\varphi_{\mathbf{r}_+} + M_{\mathbf{r}}\varphi_{\mathbf{p}}\varphi_{\mathbf{q}}, \quad (3.7b)$$

$$\partial_t \varphi_{\mathbf{r}_-}^* = (\gamma_{\mathbf{r}} + i\omega_{\mathbf{r}})\varphi_{\mathbf{r}_-}^* - M_{\mathbf{r}}^*\varphi_{\mathbf{p}}^*\varphi_{\mathbf{q}}, \quad (3.7c)$$

$$\partial_t \varphi_{\mathbf{q}} = \frac{q_x p_y}{\widehat{\alpha}_{\mathbf{q}} + q_x^2} [q_x^2(\varphi_{\mathbf{r}_+}\varphi_{\mathbf{p}}^* - \varphi_{\mathbf{r}_-}^*\varphi_{\mathbf{p}}) - i\widehat{\delta}_+(\varphi_{\mathbf{r}_+}\varphi_{\mathbf{p}}^* + \varphi_{\mathbf{r}_-}^*\varphi_{\mathbf{p}})], \quad (3.7d)$$

along with their complex-conjugate counterparts. Here,  $\widehat{\delta}_{\pm} \doteq \widehat{\delta}_{\mathbf{p}} \pm \widehat{\delta}_{\mathbf{r}}$ , and the  $M_{\mathbf{k}}$ 's are mode-coupling coefficients of the interaction between zonal flows and drift waves and are given by

$$M_{\mathbf{p}} = q_x p_y \frac{1 + p_y^2 - i\widehat{\delta}_{\mathbf{r}} - \widehat{\alpha}_{\mathbf{q}}}{1 + p_y^2 - i\widehat{\delta}_{\mathbf{p}}}, \quad (3.8a)$$

$$M_{\mathbf{r}} = q_x p_y \frac{1 - q_x^2 + p_y^2 - i\widehat{\delta}_{\mathbf{p}} - \widehat{\alpha}_{\mathbf{q}}}{1 + q_x^2 + p_y^2 - i\widehat{\delta}_{\mathbf{r}}}. \quad (3.8b)$$

It will be useful to express these coefficients in terms of their real and imaginary parts,

$$M_{\mathbf{p}}^{\text{Re}} = \frac{q_x p_y [(1 + p_y^2)^2 + \widehat{\delta}_{\mathbf{p}}\widehat{\delta}_{\mathbf{r}} - \widehat{\alpha}_{\mathbf{q}}(1 + p_y^2)]}{(1 + p_y^2)^2 + \widehat{\delta}_{\mathbf{p}}^2}, \quad (3.9a)$$

$$M_{\mathbf{p}}^{\text{Im}} = \frac{q_x p_y [\widehat{\delta}_-(1 + p_y^2) - \widehat{\alpha}_{\mathbf{q}}\widehat{\delta}_{\mathbf{p}}]}{(1 + p_y^2)^2 + \widehat{\delta}_{\mathbf{p}}^2}, \quad (3.9b)$$

$$M_{\mathbf{r}}^{\text{Re}} = \frac{q_x p_y [(1 + p_y^2)^2 - q_x^4 + \widehat{\delta}_{\mathbf{p}}\widehat{\delta}_{\mathbf{r}} - \widehat{\alpha}_{\mathbf{q}}(1 + q_x^2 + p_y^2)]}{(1 + q_x^2 + p_y^2)^2 + \widehat{\delta}_{\mathbf{r}}^2}, \quad (3.9c)$$

$$M_{\mathbf{r}}^{\text{Im}} = -\frac{q_x p_y [\widehat{\delta}_+ q_x^2 + \widehat{\delta}_-(1 + p_y^2) + \widehat{\alpha}_{\mathbf{q}}\widehat{\delta}_{\mathbf{r}}]}{(1 + q_x^2 + p_y^2)^2 + \widehat{\delta}_{\mathbf{r}}^2}. \quad (3.9d)$$

To obtain these, I have used the fact that  $\widehat{\delta}_{-\mathbf{k}} = -\widehat{\delta}_{\mathbf{k}}$ .

## 4. Numerical results

### 4.1. Setup

The nonlinear (NL) system (3.1) and quasilinear (QL) system (3.5) are simulated pseudospectrally and dealiased on a square Cartesian grid with  $L = 20\pi$  and  $N = 256$  on each side. Time stepping is performed using third-order Adams-Bashforth with an integrating factor. The vorticity at  $t = 0$  is initialized with Gaussian noise of zero mean and standard deviation  $5 \times 10^{-3}$ , with no energy in zonal modes. The random number generator used for the initial state is initialized with the same seed for all simulations. For all simulations,  $D = \mu - \nu \nabla_{\perp}^2$  where  $\mu = 1$  and  $\nu = 10^{-2}$ . To simulate the four-mode truncation, I choose modes with  $q_x = p_y = 1$  (the dependence of this system on the specific values of  $q_x$  and  $p_y$  will be understood in Sec. 5). Finally, the value of  $\beta$  at which the Dimits shift ends is denoted as a critical density gradient  $\beta^*$ . The size of the shift then is  $\Delta\beta \doteq \beta^* - \beta_{\text{lin}}$ .

I run separate simulations using the different  $\widehat{\delta}_{\mathbf{k}}$ 's given by (2.17) and (2.18),

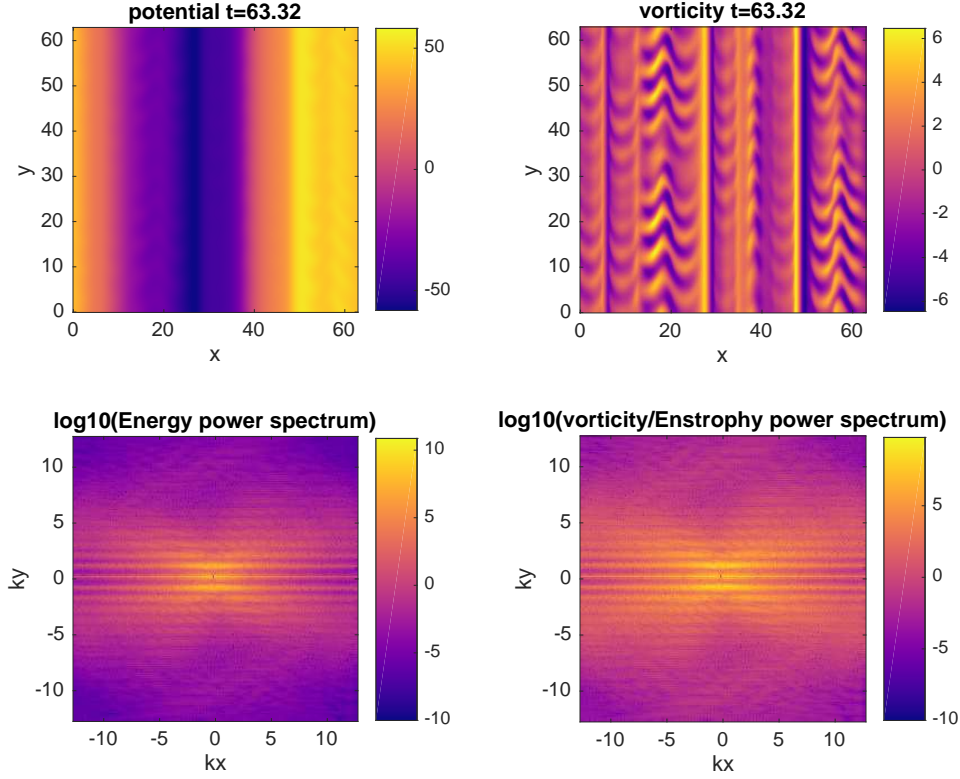


Figure 1: Snapshot of the evolution of the NL2 from direct numerical simulation with  $D = 1 - 0.01\nabla_{\perp}^2$ ,  $\beta = 5.5$  and  $\hat{\delta}_{\mathbf{k}} = 1.5ik_y$ . This value of  $\beta$  corresponds to slightly below the end of the Dimits shift. Top left displays the evolution of the potential  $\varphi$ , while the top right displays the evolution of the modified vorticity  $\zeta$ , with their respective power spectra displayed underneath.

the former with  $\delta_0 = 2$  and  $\eta_e = 0$ , and the latter with  $\delta_0 = 1.5$ . To differentiate between the two systems, I denote the former by (NL1), (QL1), etc., and the latter by (NL2), (QL2), etc. For results that are insensitive to the details of  $\hat{\delta}_{\mathbf{k}}$ , I simply use the unnumbered abbreviations. The parameters given above correspond to a threshold of linear instability at  $\beta_{\text{lin}} \approx 4.74$  for  $\hat{\delta}_{\mathbf{k}}$  given by (2.17), and  $\beta_{\text{lin}} \approx 4.21$  for  $\hat{\delta}_{\mathbf{k}}$  given by (2.18).

#### 4.2. Direct Numerical Simulation

Figure 1 contains an animation that shows the evolution of the NL2 system (3.1) with  $\hat{\delta}_{\mathbf{k}} = 1.5ik_y$  within the Dimits-shift regime ( $\beta = 5.5$ ). Additional movies with varying values of  $\beta$  for the nonlinear system ( $\beta = 4.5, 7.5$ ) as well as a movie of the quasilinear system (3.5) with  $\beta = 5.5$  are included as supplementary material, which can be accessed online. Every simulation begins with a short period of linear damping of stable drift-wave modes and linear growth of unstable ones. If the system begins below the threshold of linear instability ( $\beta < \beta_{\text{lin}}$ ) then all modes damp and the final state is the zero state; otherwise, growth of the drift-wave modes are clustered around the most unstable mode with growth rate  $\gamma = \gamma_{\text{max}}$ . Because the perturbation level at this stage is quite small ( $\varphi_{\mathbf{k}} \ll 1$ ), these modes are allowed to

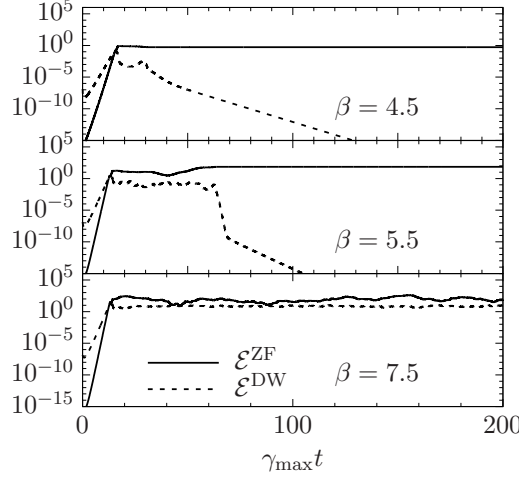


Figure 2: Direct numerical simulation of the NL2 system (3.1) with  $D = 1 - 0.01\nabla_{\perp}^2$  and  $\widehat{\delta}_{\mathbf{k}} = 1.5ik_y$  for three values of density-gradient parameter  $\beta$ . The solid line denotes the zonal component of the energy density, while the dashed line denotes the energy density in all non-zonal modes.

grow without any influence from the nonlinear interaction. As the drift-wave energy density  $\mathcal{E}^{\text{DW}}$  grows and becomes of order unity, the nonlinear interaction becomes effective in transferring energy to zonal modes, resulting in fast exponential growth in zonal energy.

Once  $\mathcal{E}^{\text{ZF}} \sim \mathcal{E}^{\text{DW}}$ , the nonlinear interaction becomes the dominant interaction for all modes and two different scenarios can take place. One possibility is for the system to find a stable zonal state that occurs after a burst of turbulent interactions (Kolesnikov and Krommes, 2005a,b). Once a stable zonal spectrum is found, the system then relaxes to a pure zonal state with the non-zonal modes damped away to zero. For simulations near the end of the Dimits shift, the system can cycle through a number of zonal spectra until finding one that is ultimately stable. The time for this to happen typically increases with  $\beta$ , though for a given realization this may not always strictly be true. The other possibility is that no such stable zonal spectrum can be reached, if it even exists. In this case the system remains in a turbulent state with finite particle flux. As an example, the nonlinear system with  $\beta = 6.5$  and  $\widehat{\delta}_{\mathbf{k}} = i\delta_0 k_y$  was run for a time of  $t = 25\,000$  without ever reaching a stable zonal state. The system with  $\widehat{\delta}_{\mathbf{k}}$  given by (2.17), on the other hand, tends to always find a stable zonal state, thus it does not exhibit a finite Dimits shift. This is further discussed below. The qualitative behaviour of both the QL system and 4MT are similar, though the quantitative aspects of the 4MT, which will be discussed, are quite different.

Figure 2 shows the evolution of both zonal and drift-wave energy densities of the NL2 system for three values of  $\beta$  versus time scaled by the respective growth rate of the fastest growing mode. The first case ( $\beta = 4.5$ ) is slightly above the threshold for linear instability. Here, the stable zonal state is found in a short time, as can be seen in the supplemental movie `DS_b5.5_NL.mp4`. The second case is near the end of the Dimits shift ( $\beta = 5.5$ ). Now the system spends significantly more time cycling through several zonal spectra until a final one is found. This is shown in

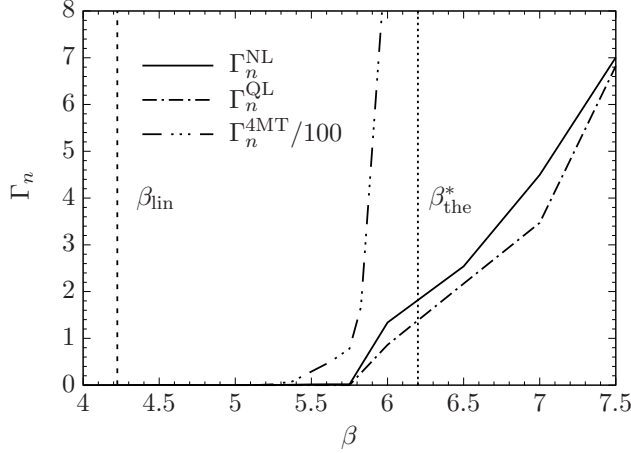


Figure 3: Particle flux for the NL2, QL2 and 4MT2 systems with  $D = 1 - 0.01\nabla_{\perp}^2$  and  $\hat{\delta}_{\mathbf{k}} = 1.5ik_y$  as a function of ion-density-gradient parameter  $\beta$ . The medium-dashed line denotes the linear threshold for instability  $\beta_{\text{lin}}$ . The dotted-line line denotes predicted end of the Dimits shift  $\beta^*$  given from the solution of (5.20).

figure 1. Finally, the third state is past the end of the Dimits shift ( $\beta = 7.5$ ). Now, the turbulent energy persists and no stable zonal state is found (see supplemental movie DS\_b7.5\_NL.mp4). These are quantitatively similar for the quasilinear system, and a representative evolution of this system is shown in the supplemental movie DS\_b5.5\_QL.mp4.

Figure 3 shows the long-time turbulent flux as a function of  $\beta$  for the NL2, QL2 and 4MT2 systems with  $\hat{\delta}_{\mathbf{k}} = 1.5ik_y$ . (This plot serves the same purpose as figure 3 in Dimits et al. 2000.) As expected, the Dimits shift is observed as a distinct lack of any flux immediately beyond the point of linear instability. Once the end of the Dimits shift is reached ( $\beta^* \approx 5.75$  for both the NL2 and QL2 systems), turbulence is again allowed to persist and turbulent transport ensues. It is important to note that the Dimits shift is quantitatively similar between the NL and the QL systems. This is a rather profound result, as the NL system contains additional avenues of energy dissipation through the direct cascade, where turbulent eddies continuously self-interact, forming smaller turbulent eddies which eventually leads to damping. On the other hand, eddies in the QL system can only be sheared via zonal flows. However, this is the dominant mechanism when the enhancement of the nonlinear zonal interaction is introduced via proper adiabatic electron response. (I shall show what this means in Sec. 5.2.3.) As a result, energy transfer is principally in the direction of  $k_x$ . This has interesting consequences, the important one being that a QL-like closure, such as CE2, suffices to capture all the relevant physics needed for the Dimits shift.

It is also important to note the discrepancy of the size of the Dimits shift, as well as the saturation levels, of the 4MT. This is simply a result of the fact that there is only a single stable mode that can accept energy. This also explains the sharp discrepancy between the saturated levels of flux between the NL/QL and 4MT; because there are far fewer stable modes, the effective damping rate is greatly reduced in the 4MT, resulting in larger levels of saturation when the system strikes

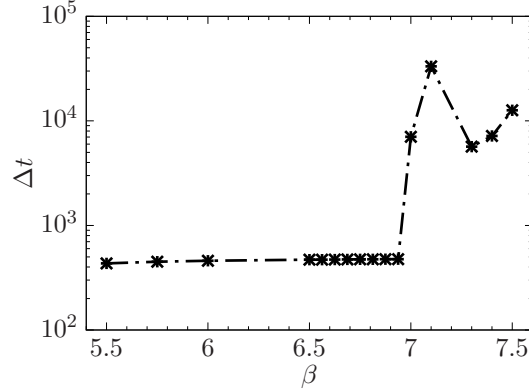


Figure 4: The time taken to reach a steady zonal state  $\Delta t$  for the NL system with  $D = 1 - 0.01\nabla_{\perp}^2$  and  $\widehat{\delta}_{\mathbf{k}}$  given by (2.17) with  $\delta_0 = 2$  and  $\eta_e = 0$  as a function of ion-density-gradient parameter  $\beta$ . Two separate regimes can clearly be seen, one where the system quickly settles into a zonal states ( $\beta < 7$ ), and one where the system takes an extended amount of time to settle ( $\beta > 7$ ).

a balance between energy production (which has not changed significantly for the 4MT as the most unstable mode is retained) and energy dissipation (which has).

I have mentioned that the system with  $\widehat{\delta}_{\mathbf{k}}$  given by (2.17) does not exhibit a finite Dimits shift; rather, a steady zonal state seems to be always found. Even so, two different regimes materialize, as shown in figure 4. Here, the time taken to reach a steady zonal state is defined as  $\Delta t \doteq t_f - t_i$ , where  $t_i$  is the first time where  $\mathcal{E}^{\text{ZF}} = \mathcal{E}^{\text{DW}}$ , and  $t_f$  is the first time where  $\mathcal{E}^{\text{DW}}/\mathcal{E}^{\text{ZF}} = 10^{-6}$ . In the first regime where  $\beta < 7$ , steady zonal states are found within  $\Delta t \sim 500$ . When  $\beta > 7$ , this time increases by at least a full order of magnitude. One possible explanation is that in the first regime, the zonal shearing associated with the Dimits shift is operational and zonal states that can sufficiently quench the drift wave turbulence are quickly found, while in the second regime additional channels of energy transfer are eventually established, thereby aiding the zonal modes to dissipate energy. The existence of the dual cascade could possibly explain the appearance of a second regime for this system, though more work is needed.

## 5. Analytical Results

I begin this section with a linear stability analysis of both the secondary and tertiary instabilities for the 4MT. With these results in hand, the size of the Dimits shift can be estimated for the fully nonlinear system, and a new understanding of the Dimits shift is gained.

### 5.1. Zonal growth rates of the secondary instability

At the beginning of the simulation, the most unstable drift-wave mode grows without any influence from the zonal or side-band modes in what I shall call the secondary-instability regime. One can then solve (3.7b-d) with  $\varphi_{\mathbf{p}} = \varphi_0 e^{(\gamma_{\mathbf{p}} + i\omega_{\mathbf{p}})t}$ ,

which renders the remaining equations a linear system:

$$\partial_t \varphi_{\mathbf{r}_+} = (\gamma_{\mathbf{r}} - i\omega_{\mathbf{r}})\varphi_{\mathbf{r}_+} + M_{\mathbf{r}}\varphi_0 e^{\gamma_{\mathbf{p}}t - i\omega_{\mathbf{p}}t} \varphi_{\mathbf{q}}, \quad (5.1a)$$

$$\partial_t \varphi_{\mathbf{r}_-}^* = (\gamma_{\mathbf{r}} + i\omega_{\mathbf{r}})\varphi_{\mathbf{r}_-}^* - M_{\mathbf{r}}^* \varphi_0^* e^{\gamma_{\mathbf{p}}t + i\omega_{\mathbf{p}}t} \varphi_{\mathbf{q}}, \quad (5.1b)$$

$$\begin{aligned} \partial_t \varphi_{\mathbf{q}} = & \frac{q_x p_y e^{\gamma_{\mathbf{p}}t}}{\widehat{\alpha}_{\mathbf{q}} + q_x^2} [q_x^2 (\varphi_{\mathbf{r}_+} \varphi_0^* e^{i\omega_{\mathbf{p}}t} - \varphi_{\mathbf{r}_-}^* \varphi_0 e^{-i\omega_{\mathbf{p}}t}) \\ & - i\widehat{\delta}_+ (\varphi_{\mathbf{r}_+} \varphi_0^* e^{i\omega_{\mathbf{p}}t} + \varphi_{\mathbf{r}_-}^* \varphi_0 e^{-i\omega_{\mathbf{p}}t})]. \end{aligned} \quad (5.1c)$$

The goal is now to determine the growth rate of the zonal flow against this growing drift wave mode.

At this point, one can make a further approximation by focusing on the region where the zonal mode grows much faster than the drift-wave mode, making the assumption  $\gamma_{\mathbf{p}} = \gamma_{\mathbf{r}} = 0$ . Alternatively one can also proceed, without any further assumptions, to derive an evolution equation for  $\varphi_{\mathbf{q}}$ ; this is done here.

To do so, the transformations  $\varphi_{\mathbf{r}_+} = \varphi_0 \varphi'_{\mathbf{r}_+} e^{-i\omega_{\mathbf{p}}t}$  and  $\varphi_{\mathbf{r}_-}^* = \varphi_0^* \varphi'^*_{\mathbf{r}_-} e^{i\omega_{\mathbf{p}}t}$  are made to eliminate the rapid oscillatory behaviour of the drift-wave mode. New equations of motion are then formulated for the variables  $\Lambda_{\pm} \doteq \varphi'_{\mathbf{r}_{\pm}} \pm \varphi'^*_{\mathbf{r}_{\pm}}$ . Defining  $\gamma_{\pm} \doteq \gamma_{\mathbf{p}} \pm \gamma_{\mathbf{r}}$  and  $\omega_{\pm} \doteq \omega_{\mathbf{p}} \pm \omega_{\mathbf{r}}$ , (3.7a–c) become

$$\partial_t \Lambda_+ = \gamma_{\mathbf{r}} \Lambda_+ - i\omega_- \Lambda_- + 2iM_{\mathbf{r}}^{\text{Im}} e^{\gamma_{\mathbf{p}}t} \varphi_{\mathbf{q}}, \quad (5.2a)$$

$$\partial_t \Lambda_- = \gamma_{\mathbf{r}} \Lambda_- - i\omega_- \Lambda_+ + 2M_{\mathbf{r}}^{\text{Re}} e^{\gamma_{\mathbf{p}}t} \varphi_{\mathbf{q}}, \quad (5.2b)$$

$$\partial_t \varphi_{\mathbf{q}} = \frac{|\varphi_0|^2 q_x p_y e^{\gamma_{\mathbf{p}}t}}{\widehat{\alpha}_{\mathbf{q}} + q_x^2} \left( q_x^2 \Lambda_- - i\widehat{\delta}_+ \Lambda_+ \right). \quad (5.2c)$$

From here, it is a simple exercise to derive an ordinary differential equation for the zonal mode by combining (5.2a–c):

$$\varphi_{\mathbf{q}}''' - A\varphi_{\mathbf{q}}'' + (B - Ce^{2\gamma_{\mathbf{p}}t})\varphi_{\mathbf{q}}' - De^{2\gamma_{\mathbf{p}}t}\varphi_{\mathbf{q}} = 0, \quad (5.3)$$

where

$$A = 2\gamma_+, \quad (5.4a)$$

$$B = \omega_-^2 + \gamma_+^2, \quad (5.4b)$$

$$C = \frac{2|\varphi_0|^2 q_x p_y}{\widehat{\alpha}_{\mathbf{q}} + q_x^2} \left( q_x^2 M_{\mathbf{r}}^{\text{Re}} + \widehat{\delta}_+ M_{\mathbf{r}}^{\text{Im}} \right), \quad (5.4c)$$

$$D = \frac{2|\varphi_0|^2 q_x p_y}{\widehat{\alpha}_{\mathbf{q}} + q_x^2} \left[ \gamma_- \left( q_x^2 M_{\mathbf{r}}^{\text{Re}} + \widehat{\delta}_+ M_{\mathbf{r}}^{\text{Im}} \right) + \omega_- \left( q_x^2 M_{\mathbf{r}}^{\text{Im}} - \widehat{\delta}_+ M_{\mathbf{r}}^{\text{Re}} \right) \right]. \quad (5.4d)$$

The usual dispersion relation of the modulational instability for the HME is recovered by setting  $\widehat{\delta}_{\mathbf{k}} = 0$  and  $\widehat{\alpha}_{\mathbf{q}} = 1$  (Connaughton et al., 2010).

The goal is to analyze (5.3) in the asymptotic limits  $t \rightarrow 0$  and  $t \rightarrow \infty$ . The latter, however, is made difficult by the fact that  $C, D \propto |\varphi_0^2| \lll 1$ . Furthermore,  $C$  and  $D$  can be of different orders *relative to each other*, exacerbating the situation. The limit  $t \rightarrow \infty$  cannot be taken at face value then, as this asymptotic time may occur well beyond the range of validity of this approximation (that is to say, beyond the secondary-instability regime). Thus, (5.3) must be analyzed in the asymptotic limit  $t \rightarrow \infty$ , which is coarse-grained according to the relative size of the coefficients  $A, B, C$  and  $D$ , based on a given set of parameters  $q_x, p_y$  and  $\beta$ .

For  $t \rightarrow 0$ , the  $C$  and  $D$  coefficients become subdominant. The resulting equation

is solved readily,

$$y \sim \exp \left[ t \left( A \pm \sqrt{A^2 - 4B} \right) / 2 \right], \quad (5.5)$$

and  $y \sim c$  where  $c$  is a constant. The last solution is the one pertaining to the zonal mode, while the other two are related to the linear evolution of the sideband modes.

To analyze the limit  $t \rightarrow \infty$ , the Ansatz  $\varphi_{\mathbf{q}} \sim e^{S(t)}$  is used in (5.3), resulting in

$$S''' + 3S''S' + S'^3 - A(S'' + S'^2) + (B - e^{2\gamma_{\mathbf{p}}t}C)S' - e^{2\gamma_{\mathbf{p}}t}D = 0. \quad (5.6)$$

Two cases are now considered. First, let both  $C$  and  $D$  be of the same order. One then finds the leading order behaviours  $\varphi_{\mathbf{q}} \sim \exp(-Dt/C)$  and

$$\varphi_{\mathbf{q}} \sim \exp(\pm ae^{\gamma_{\mathbf{p}}t} + bt), \quad (5.7)$$

where

$$a = \sqrt{C}/\gamma_{\mathbf{p}}, \quad (5.8a)$$

$$b = (AC + D - 3\gamma_{\mathbf{b}}C)/2C. \quad (5.8b)$$

These apply equally well to the case where  $D \rightarrow 0$ . For the other case where  $C$  is subdominant, one finds the leading order behaviour

$$\varphi_{\mathbf{q}} \sim \exp(I_3 a' e^{2\gamma_{\mathbf{p}}t/3} + b't), \quad (5.9)$$

where

$$a' = \frac{3D^{1/3}}{2\gamma_{\mathbf{p}}}, \quad (5.10a)$$

$$b' = (A - 2\gamma_{\mathbf{b}})/3, \quad (5.10b)$$

and  $I_3$  is a cube root of unity. Both (5.7) and (5.9) represent instabilities of Kelvin-Helmholtz type ( $\gamma \sim |q_x p_y \varphi_{\mathbf{p}}|^\varepsilon \sim |q_x v_x|^\varepsilon$  where  $\varepsilon$  is a constant of order unity). This agrees with the usual picture of the secondary instability given by Rogers et al. (2000).

Again, it is emphasized that which asymptotic behaviour is relevant depends on the specific values of  $q_x$ ,  $p_y$ , and  $\beta$ , as well as where the kinematic regime ends. For instance, with  $q_x = 0.6$ ,  $p_y = 1.3$  and  $\beta = 5$ ,  $C$  is subdominant for  $t \lesssim 200$ , and so the second situation applies. Figure 5 shows the evolution of the drift-wave energy and the zonal energy for the 4MT with  $\beta = 5$ . Both the numerical solution of (5.3) and the scaling given by (5.9) are displayed, showing excellent agreement.

Unfortunately, it is difficult to extend this analysis to the NL or QL systems in order to determine the dominant zonal mode, as the cumulative effect of the asymptotic behaviour of every mode is somewhat unclear. Even then, such a prediction would only predict a dominant zonal mode *during the initial kinematic stage*. There is no *a priori* reason why this mode would remain the dominant one once the fully-nonlinear interaction stage comes to an end. More sophisticated approaches, such as the wave-kinetic equation (Diamond et al., 2005; Ruiz et al., 2016), have been used in the past to calculate zonal growth rates with some success. However, this approach assumes a homogeneous background of drift-wave turbulence (Krommes and Kim, 2000), which isn't the case in this regime. The zonal flows are also assumed to be quasi-static (Parker, 2016), an assumption that breaks down during the short turbulent interaction phase of the Dimits shift, so the usefulness of the

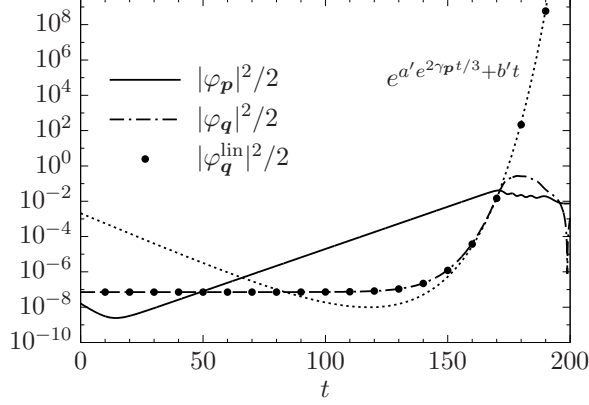


Figure 5: Typical energy evolution for the 4MT system as described in Sec. 5.1 with  $q_x = 0.6$ ,  $p_y = 1.3$ ,  $D = 1 - 0.01\nabla_{\perp}^2$ ,  $\beta = 5$  and  $\hat{\delta}_{\mathbf{k}}$  given by (2.17) with  $\delta_0 = 2$  and  $\eta_e = 0$ . The solid line denotes the drift-wave mode energy while the dot-dashed line denotes the zonal mode energy. The numerical solution to (5.3) is plotted with points, with the  $t \rightarrow \infty$  asymptotic behaviour being shown as a dotted line.

wave-kinetic equation for calculating zonal growth rates of the secondary instability during the Dimits shift is at this point uncertain.

### 5.2. Zonal mode stability analysis of the tertiary instability

This calculation can be repeated to study the stability of a zonal mode to a drift-wave perturbation, otherwise known as the tertiary instability. A similar calculation has been performed in Rogers et al. (2000) where those authors dealt with the ITG mode. For a background zonal state  $\varphi_q = \varphi_0$ , the linearized equations of motion are

$$\partial_t \varphi_{\mathbf{p}} = \lambda_{\mathbf{p}} \varphi_{\mathbf{p}} + M_{\mathbf{p}}(\varphi_0 \varphi_{\mathbf{r}_-} - \varphi_0^* \varphi_{\mathbf{r}_+}), \quad (5.11a)$$

$$\partial_t \varphi_{\mathbf{r}_+} = \lambda_{\mathbf{r}_+} \varphi_{\mathbf{r}_+} + M_{\mathbf{r}} \varphi_{\mathbf{p}} \varphi_0, \quad (5.11b)$$

$$\partial_t \varphi_{\mathbf{r}_-} = \lambda_{\mathbf{r}_-} \varphi_{\mathbf{r}_-} - M_{\mathbf{r}} \varphi_{\mathbf{p}} \varphi_0^*. \quad (5.11c)$$

The eigenvalues are quickly found:  $\lambda = (\gamma_{\mathbf{r}} - i\omega_{\mathbf{r}})$  and

$$\lambda_{\pm} = \frac{1}{2} \left[ \lambda_{\mathbf{p}} + \lambda_{\mathbf{r}} \pm \left( (\lambda_{\mathbf{p}} - \lambda_{\mathbf{r}})^2 - 8|\varphi_0|^2 M_{\mathbf{p}} M_{\mathbf{r}} \right)^{1/2} \right]. \quad (5.12)$$

The destabilizing root is the positive branch which has the real component

$$\text{Re}(\lambda_+) = \frac{1}{2} \left[ \gamma_+ + \sqrt{\frac{1}{2} \left( \Omega + \sqrt{\Omega^2 + \Theta^2} \right)^{1/2}} \right], \quad (5.13)$$

where

$$\Omega \doteq \gamma_-^2 - \omega_-^2 - 8|\varphi_0|^2 (M_{\mathbf{p}}^{\text{Re}} M_{\mathbf{r}}^{\text{Re}} - M_{\mathbf{p}}^{\text{Im}} M_{\mathbf{r}}^{\text{Im}}), \quad (5.14)$$

$$\Theta \doteq 2\omega_- \gamma_- + 8|\varphi_0|^2 (M_{\mathbf{p}}^{\text{Re}} M_{\mathbf{r}}^{\text{Im}} + M_{\mathbf{p}}^{\text{Im}} M_{\mathbf{r}}^{\text{Re}}). \quad (5.15)$$

Immediately, certain terms appear with physical importance. For instance,  $\omega_-$  represents the modulational part of the dispersion relation that is due to dispersive effects, while  $\gamma_+$  is the coupling of the linear growth rates by the nonlinear interaction.



Equation (5.13) contains a wealth of information that must be carefully parsed. This shall be done in subsections.

*5.2.1. Maximally-Coupled Modes* When the outer discriminant of (5.13) vanishes, the real part of both the unstable and stable eigenvalues becomes  $\text{Re}(\lambda_+) = \gamma_+/2$ . This corresponds to a special situation where both the drift-wave and sideband modes become maximally coupled, and occurs when  $\Theta = 0$  and  $\Omega \leq 0$ . Here, both modes work together in tandem to create a coupled mode with an effective damping rate that is the average of the individual growth rates. This coupled mode will be referred to as the Maximally-Coupled Mode (MCM). In principle, MCMs can exist for arbitrary drift-wave/sideband pairings where the primary drift-wave mode contains a non-zero component along  $k_x$ . However, for the rest of this discussion I make the approximation that for the quantitative aspects of the Dimits shift, only the most unstable drift-wave mode (which must be purely radial with wavenumber  $p_y^*$ ) is relevant.

The upper bound of the Dimits shift for the 4MT can then be quickly found as the solution to the equation  $\gamma_+ = 0$ , or

$$\beta^* = \frac{(D_{\mathbf{p}} + D_{\mathbf{r}})}{p_y} \frac{[(1 + p_y^2)^2 + \widehat{\delta}_{\mathbf{p}}^2][(1 + q_x^2 + p_y^2)^2 + \widehat{\delta}_{\mathbf{r}}^2]}{\widehat{\delta}_{\mathbf{r}}[(1 + p_y^2)^2 + \widehat{\delta}_{\mathbf{p}}^2] + \widehat{\delta}_{\mathbf{p}}[(1 + q_x^2 + p_y^2)^2 + \widehat{\delta}_{\mathbf{r}}^2]}. \quad (5.16)$$

This predicts the end of the Dimits shift for the system considered in Sec. 4.2 to be  $\beta^* = 5.2$ , in excellent agreement with the simulation result in figure 3.

*5.2.2. The most stable zonal amplitude* In order to develop MCMs, the condition  $\Theta = 0$  must be satisfied. There then exists a zonal amplitude that is most stable, given by

$$|\varphi_0|^2 = -\frac{\omega_- \gamma_-}{4(M_{\mathbf{p}}^{\text{Re}} M_{\mathbf{r}}^{\text{Im}} + M_{\mathbf{p}}^{\text{Im}} M_{\mathbf{r}}^{\text{Re}})}. \quad (5.17)$$

The stability of such a mode has been verified numerically. Two important special cases are now apparent. If  $\omega_- = 0$  and  $M_{\mathbf{p}}^{\text{Im}}, M_{\mathbf{r}}^{\text{Im}} \neq 0$ , then no amount of zonal amplitude is stabilizing, thus the frequency mismatch between drift-wave and sideband modes is needed to stabilize the zonal mode. However, if  $M_{\mathbf{p}}^{\text{Im}} = M_{\mathbf{r}}^{\text{Im}} = 0$  and  $\omega_- \neq 0$  (as would be the case if linear instability was introduced by hand without modifying the Poisson equation) then maximal coupling can only be achieved with  $\varphi_0 \rightarrow \infty$ . Finally, if  $M_{\mathbf{p}}^{\text{Im}} = M_{\mathbf{r}}^{\text{Im}} = \omega_- = 0$ , then any amount of zonal amplitude is stabilizing. Additional zonal amplitude beyond a certain limit, however, ceases to make any further difference.

*5.2.3. The zonal Kelvin-Helmholtz instability* The other condition that must be satisfied is  $\Omega < 0$ . Here, the modulational instability that materializes as  $\omega_-$  is a stabilizing effect. More importantly, however, is that

$$M_{\mathbf{p}}^{\text{Re}} M_{\mathbf{r}}^{\text{Re}} - M_{\mathbf{p}}^{\text{Im}} M_{\mathbf{r}}^{\text{Im}} > 0. \quad (5.18)$$

It is important to realize that  $M_{\mathbf{k}} \sim q_x p_y$  times a factor of order unity. This term then clearly represents a Kelvin-Helmholtz-type destabilization of the zonal mode, and can become dominant for sufficiently large zonal amplitudes and negative values of the mode-coupling factor. However, this term only needs to be comparable to  $\gamma_-^2 - \omega_-^2$  in order to spoil the coupling between drift-wave modes. This happens for

a sufficiently large value of  $q_x$  (denoted by  $q_x^*$ ) and signifies the smallest scale where the last MCM is formed.

I now make clear what is meant when I say that the introduction of the  $\hat{\alpha}$  operator to the Poisson equation results in a boost to the nonlinear zonal interaction. Consider the mode-coupling coefficients of the HME ((3.8) with  $\hat{\delta}_{\mathbf{k}} = 0$  and  $\hat{\alpha}_{\mathbf{q}} = 1$ ). Solution of  $M_{\mathbf{p}}^{\text{Re}} M_{\mathbf{r}}^{\text{Re}} = M_{\mathbf{p}}^{\text{Im}} M_{\mathbf{r}}^{\text{Im}} \equiv 0$  leads to the Kelvin-Helmholtz stability threshold of  $q_x^* = p_y^*$ , implying local zonal interaction. However, the  $\hat{\alpha}$  operator in the mHME (viz. (3.8) with  $\hat{\delta}_{\mathbf{k}} = 0$  and  $\hat{\alpha}_{\mathbf{q}} = 0$ ) leads to the stability threshold

$$q_x^{*2} = 1 + p_y^{*2}. \quad (5.19)$$

Typically,  $p_y^* \ll 1$  in toroidal plasmas, leading to  $q_x^*$  and  $p_y^*$  that are of disparate scales. This is a rather surprising result, as this means that the energy transfer caused by zonal shearing can be *non-local*. This example illustrates the fact that this boost materializes as an increase in the range of radial scales where MCMs can develop, emphasizing the importance of contributions from small-scale zonal flows. Even when  $p_y^* \sim 1$ , this slight increase in range can still lead to dramatic effects. This is in stark contrast to the scale-by-scale transfer due to the Kolmogorov-type cascade with a transfer rate that is limited by the local eddy turnover time.

### 5.3. Estimation of the Dimits shift

Motivated by the numerical results presented in Sec. 4.2, I now leverage the above calculations to make an estimate of the Dimits shift for the fully nonlinear system, giving new insights into the nature of the tertiary instability. The physical picture is as follows: as zonal flows are generated from the secondary instability, drift-waves become sheared, resulting in a direct transfer of energy to smaller scales. As energy flow is principally horizontal in  $k$  space (i.e. energy is not transferred between bands with different  $k_y$ ), the relevant value of  $p_y$  that determines stability is that given by the most unstable drift-wave mode, denoted by  $p_y^*$ . This transfer can only be done efficiently down to the scale given by  $q_x^*$ , as the Kelvin-Helmholtz-type destabilization acts to spoil the coupling between drift waves to this scale. This is the last point where energy generated by the most unstable mode can be efficiently transferred through an MCM. Thus the Dimits shift will roughly terminate when the last MCM at this scale itself becomes unstable.

Quantitatively, this situation can be described as a system of four equations,

$$\left. \frac{\partial \gamma_{\mathbf{p}}}{\partial p_y} \right|_{p_y=p_y^*} = 0, \quad (5.20a)$$

$$\Theta = 0, \quad (5.20b)$$

$$\Omega = 0, \quad (5.20c)$$

$$\gamma_+(q_x^*, p_y^*) = 0, \quad (5.20d)$$

and four unknowns  $q_x^*$ ,  $p_y^*$ ,  $|\varphi_0|^2$ , and  $\beta^*$ . The first equation relates  $p_y^*$  of the most unstable drift-wave mode to the instability parameter  $\beta^*$ . The second equation determines the most-stable zonal amplitude for the given triad and relates  $|\varphi_0|^2$ ,  $q_x^*$ , and  $p_y^*$ . The third equation gives the point at which the zonal mode cannot efficiently couple drift-wave modes and relates  $|\varphi_0|^2$ ,  $q_x^*$ , and  $p_y^*$ . Finally, the last equation indicates the point where the last MCM becomes unstable and relates  $q_x^*$ ,  $p_y^*$ , and  $\beta^*$ .

Numerical solution of this system of equations with  $\hat{\delta}_{\mathbf{k}} = 1.5k_y$  and  $D = 1 -$

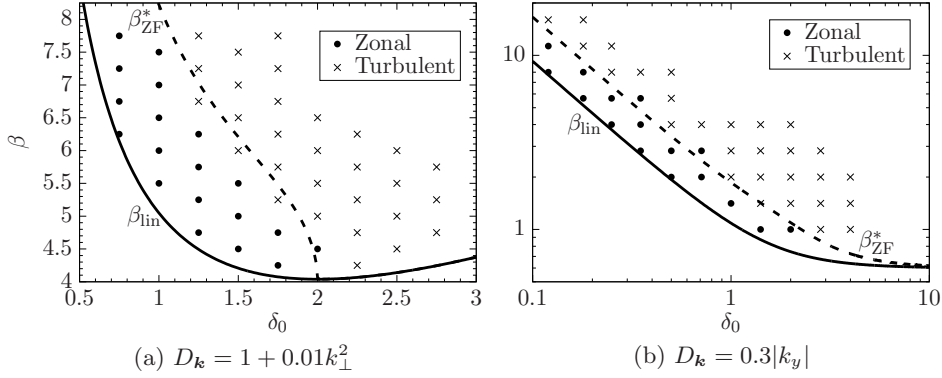


Figure 6: Parameter scan of the nonlinear system with  $\widehat{\delta}_{\mathbf{k}}$  given by (2.17). The left panel (a) uses  $D_{\mathbf{k}} = 1 + 0.01k_{\perp}^2$ , while the right panel (b) uses  $D_{\mathbf{k}} = 0.3|k_y|$ . Bold dots denote system that end in steady zonal states while crosses denote systems that end in turbulent states. The solid line marks the linear stability threshold, while the dashed line denotes the predicted end of the Dimits shift  $\beta^*$  given from the solution of (5.20).

$0.01\nabla_{\perp}^2$  yields  $\beta^* \approx 6.2$  and results in a Dimits shift size of  $\Delta\beta \approx 2.0$ . This is within the value obtained by the direct numerical simulation in Sec. 4.2 ( $\beta^* \gtrsim 5.75$  and  $\Delta\beta \approx 1.5$ ) by roughly 25%. This is a fairly good estimate, considering it is the result of a straightforward linear calculation with only a few nonlinear considerations. Notice that this analysis is insensitive to the details of the underlying model; it applies equally well to *any* Hasegawa-Mima-like equation, and should be generalizable to more complicated ones, such as the two-field ITG and Hasegawa-Wakatani models. I stress that this is only an estimate; it is neither an upper bound, as additional avenues of efficient energy transfer may exist, nor is it a lower bound, as the existence of a stable state does not guarantee it is physically realizable.

Figure 6 shows a parameter scan of the system with  $\widehat{\delta}_{\mathbf{k}} = i\delta_0 k_y$  over both  $\delta_0$  and  $\beta$ . The left panel (a) uses frictional and viscous damping with  $D_{\mathbf{k}} = 1 + 0.01k_{\perp}^2$ , while the right panel (b) uses a damping operator appropriate for a Landau-fluid closure with  $D_{\mathbf{k}} = 0.3|k_y|$ . These simulations are run for a maximum time of  $t = 10\,000$ . Bold dots denote simulations that end in steady zonal states while crosses denote systems that end with turbulence. The solid line shows the linear stability threshold while the dashed line shows the threshold calculated from (5.20). This plot shows good agreement between the estimation and the observed numerical boundary of the Dimits shift. Surprisingly, in panel (a) the estimation also reasonably predicts the boundary at  $\delta_0 = 2$ .

One important caveat to this estimation is it must be modified somewhat when applied to a system with a strong dual cascade. In addition to nonlocal transfer from the zonal flows, there can also be transfer to *large scales* that can lead to dissipation by large-scale sinks. If the coupling to these modes is efficient, then the Dimits shift could possibly be extended. A correction can then be made to the above analysis by assuming maximal coupling between the most unstable drift-wave mode and the most unstable mode at the box scale, which is typically purely radial with wavevector  $\mathbf{p}^{\text{box}} \doteq (0, 2\pi/L_y)$ . Then two critical values of  $\beta^*$  must be calculated,

one due to the zonal interaction (denoted by  $\beta_{ZF}^*$ ) and the other due to the inverse cascade (denoted by  $\beta_{IC}^*$ ). The latter value is given by the solution to the system of equations

$$\left. \frac{\partial \gamma_{\mathbf{p}}}{\partial p_y} \right|_{p_y=p_y^*} = 0, \quad (5.21a)$$

$$\gamma_{\mathbf{p}^*} + \gamma_{\mathbf{p}^{\text{box}}} = 0. \quad (5.21b)$$

If the inverse cascade can achieve maximal coupling, then the new critical density gradient would be  $\beta^* = \text{Max}(\beta_{ZF}^*, \beta_{IC}^*)$ . Otherwise, the best one can do without further analysis is to confine the critical density gradient within the interval  $\beta_{ZF}^* \leq \beta^* \leq \text{Max}(\beta_{ZF}^*, \beta_{IC}^*)$ . The system considered in Sec. 4.2 with  $\hat{\delta}_{\mathbf{k}}$  given by (2.17) with  $L_y = 20\pi$  leads to  $\beta_{ZF}^* \approx 7.25$  and  $\beta_{IC}^* \approx 9.4$ , which lends further credence to the existence of an inverse cascade. While it would be desirable to show that no steady zonal state exists beyond this critical gradient, such simulations become unfeasible as they would have to be run over an extended period of time, even beyond those witnessed in figure 4. This will be left for future exploration.

Finally, this analysis says nothing about the possibility of coupling of modes on stable and unstable branches at similar points in  $k$  space (see the recent work of Makwana et al. 2014). This coupling does not exist in the present one-field model, but this may be important when extending the analysis to the gyrokinetic equation.

## 6. Discussion and Conclusion

I have shown through direct numerical simulation that the Terry-Horton equation can be made to exhibit the Dimits shift with two suitable modifications. First, proper adiabatic electron response is added to ensure that electrons do not respond to a potential that is constant along a flux surface. Secondly, zonal modes are made to be explicitly undamped, thus capturing the residual Rosenbluth-Hinton states seen in gyrokinetic simulations. This phenomenon persists after various simplifications. Analytical progress was made on a four-mode truncation of the system, focusing on the behaviour of the zonal mode growth during the secondary instability, and calculating an upper bound on the end of the Dimits shift. Importantly, it was shown here that the system can only efficiently couple modes down to a scale set by a Kelvin-Helmholtz-type destabilization. Using this information, the size of the Dimits shift was estimated for the nonlinear system and an intuitive picture of the underlying mechanism emerged, providing new insights. In particular, the role of small scale zonal flows was found to be an important mechanism of energy transfer within the Dimits shift.

I reiterate that the goal of this model is to serve as a proving ground for analytical techniques that can be used to quantify the shift in more complete systems. I also believe this model possesses pedagogical merits as well. The model itself is transparent and self-contained; the calculations presented in this article are simple and intuitive, yet illuminating. One can then learn about the essential aspects of the Dimits shift without needing to go into the methodology of gyrokinetics and geometry, and can be used as a stepping stone to more difficult and relevant problems.

Future work should focus on extending this analysis to more physically complete (e.g., gyrokinetic) systems to see if one can derive the size of shift originally seen

for the Cyclone Base Case in Dimits et al. (2000). Other quantities of interest are the saturation levels and spectra of the zonal flows resulting from the secondary instability, and the saturation levels of turbulent transport beyond the shift.

Finally, a better estimate of the size of the Dimits shift for the mTHE should be derived using more rigorous methods. This can be done, in principle, by using statistical closures to study the nonlinear mechanisms. However, as Krommes and Parker (2015) have pointed out, it is necessary to begin with an inhomogeneous closure in order that one can consider inhomogeneous symmetry-breaking perturbations (zonal flows) to a state of homogeneous turbulence. (As was discussed by St-Onge and Krommes 2017, here ‘turbulence’ below the point of zonal instability refers to homogeneous noise due to discrete particles.) Not only does an inhomogeneous closure allow for symmetry breaking, it contains all of the physical effects involved in destabilizing those flows and allowing for a transition from the Dimits-shift regime to states of fully developed turbulence. Because the general structure of an inhomogeneous closure is necessarily complicated, carrying out such a program to completion represents a significant challenge for the future.

#### Acknowledgements

I would like to thank J. A. Krommes, G. W. Hammett, and T. Stoltzfus-Dueck for many instructive discussions. I would also like to thank J. B. Parker and J. Squire for help with the numerics. Finally, I would like to thank M. W. Kunz for his steadfast and unwavering support of this research. This work was supported by U.S. DoE contract DE-AC02-09CH11466.

#### References

- M. A. Beer and G. W. Hammett. The dynamics of small-scale turbulence-driven flows. In *Proc. of the Joint Varenna-Lausanne Int. Workshop on Theory of Fusion Plasmas*, 1998.
- K. H. Burrell. Effects of  $\mathbf{E} \times \mathbf{B}$  velocity shear and magnetic shear on turbulence and transport in magnetic confinement devices. *Physics of Plasmas*, 4(5):1499–1518, 1997.
- C. P. Connaughton, B. T. Nadiga, S. V. Nazarenko, and B. E. Quinn. Modulational instability of Rossby and drift waves and generation of zonal jets. *J. Fluid Mech.*, 654:207231, 2010.
- P. H. Diamond, S-I Itoh, K. Itoh, and T. S. Hahm. Zonal flows in plasma - a review. *Plasma Physics and Controlled Fusion*, 47(5):R35, 2005.
- A. M. Dimits, D. E. Shumaker, W. M. Nevins, B. I. Cohen, and S. E. Parker. Raised nonlinear thresholds and numerical convergence in gyrokinetic simulations of ion-temperature-gradient turbulence in tokamaks. International Sherwood Fusion Theory Conference, Atlanta, GA, 1998.
- A. M. Dimits, G. Bateman, M. A. Beer, B. I. Cohen, W. Dorland, G. W. Hammett, C. Kim, J. E. Kinsey, M. Kotschenreuther, A. H. Kritz, L. L. Lao, J. Mandrekas, W. M. Nevins, S. E. Parker, A. J. Redd, D. E. Shumaker, R. Sydora, and J. Weiland. Comparisons and physics basis of tokamak transport models and turbulence simulations. *Physics of Plasmas*, 7(3):969–983, 2000.
- B. F. Farrell and P. J. Ioannou. A stochastic structural stability theory model of the drift wave–zonal flow system. *Physics of Plasmas*, 16(11):112903, 2009.
- G. W. Hammett, M. A. Beer, W. Dorland, S. C. Cowley, and S. A. Smith. Devel-

- opments in the gyrofluid approach to tokamak turbulence simulations. *Plasm. Phys. Control. Fus.*, 35:973, 1993.
- R. A. Kolesnikov and J. A. Krommes. Transition to collisionless ion-temperature-gradient-driven plasma turbulence: A dynamical systems approach. *Phys. Rev. Lett.*, 94:235002, Jun 2005a.
- R. A. Kolesnikov and J. A. Krommes. Bifurcation theory of the transition to collisionless ion-temperature-gradient-driven plasma turbulence. *Physics of Plasmas*, 12(12):122302, 2005b.
- J. A. Krommes and J. B. Parker. Statistical closures and zonal flows. In B. Galperin and P. Read, editors, *Zonal Jets*, chapter V.1.1. Cambridge University Press, Cambridge, 2015. in press.
- John A. Krommes and Chang-Bae Kim. Interactions of disparate scales in drift-wave turbulence. *Phys. Rev. E*, 62:8508–8539, 2000.
- Y.-M. Liang, P. H. Diamond, X.-H. Wang, D. E. Newman, and P. W. Terry. A two-nonlinearity model of dissipative drift wave turbulence. *Physics of Fluids B: Plasma Physics*, 5(4):1128–1139, 1993.
- Z. Lin, T. S. Hahm, W. W. Lee, W. M. Tang, and P. H. Diamond. Effects of collisional zonal flow damping on turbulent transport. *Phys. Rev. Lett.*, 83:3645–3648, Nov 1999.
- K. D. Makwana, P. W. Terry, M. J. Pueschel, and D. R. Hatch. Subdominant modes in zonal-flow-regulated turbulence. *Phys. Rev. Lett.*, 112:095002, Mar 2014.
- R. Numata, R. Ball, and R. L. Dewar. Bifurcation in electrostatic resistive drift wave turbulence. *Physics of Plasmas*, 14(10):102312, 2007.
- M. Ottaviani, M.A. Beer, S.C. Cowley, W. Horton, and J.A. Krommes. Turbulence and intermittency in plasmas unanswered questions in ion-temperature-gradient-driven turbulence. *Physics Reports*, 283(1):121–146, 1997. ISSN 0370-1573.
- J. B. Parker. Dynamics of zonal flows: Failure of wave-kinetic theory, and new geometrical optics approximations. *Journal of Plasma Physics*, 82(6), 2016.
- J. B. Parker and J. A. Krommes. Zonal flow as pattern formation. *Physics of Plasmas*, 20(10):100703, 2013.
- J. B. Parker and J. A. Krommes. Generation of zonal flows through symmetry breaking of statistical homogeneity. *New Journal of Physics*, 16(3):035006, 2014.
- B. N. Rogers, W. Dorland, and M. Kotschenreuther. Generation and stability of zonal flows in ion-temperature-gradient mode turbulence. *Phys. Rev. Lett.*, 85:5336, 2000.
- M. N. Rosenbluth and F. L. Hinton. Poloidal flow driven by ion-temperature-gradient turbulence in tokamaks. *Phys. Rev. Lett.*, 80:724–727, Jan 1998.
- D. E. Ruiz, J. B. Parker, E. L. Shi, and I. Y. Dodin. Zonal-flow dynamics from a phase-space perspective. *Physics of Plasmas*, 23(12):122304, 2016.
- K. Srinivasan and W. R. Young. Zonostrophic instability. *Journal of the Atmospheric Sciences*, 69(5):1633–1656, 2012.
- D. A. St-Onge and J. A. Krommes. Zonostrophic instability driven by discrete particle noise. *Physics of Plasmas*, 24(4):042107, 2017.
- W.M. Tang. Microinstability theory in tokamaks. *Nuclear Fusion*, 18(8):1089, 1978.
- P. W. Terry and W. Horton. Stochasticity and the random phase approximation for three electron drift waves. *Phys. Fluids*, 25(491), 1982.
- P. W. Terry and W. Horton. Drift wave turbulence in a low-order  $k$  space. *Phys. Fluids*, 26(106), 1983.